Ionization of Stark states with half-cycle pulses: Interference effects in the continuum

Corneliu Manescu,[1] Jeffrey L. Krause,[1] and Kenneth J. Schafer[2]
[1]*Quantum Theory Project, University of Florida, Gainesville, Florida 32611-8435, USA*
[2]*Department of Physics and Astronomy, Louisiana State University, Baton Rouge, Louisiana 70803-4001, USA*
(Received 17 October 2002; published 11 July 2003)

We study the ionization of extreme Stark states in sodium by THz electromagnetic half-cycle pulses. The results of our full-quantum calculations reveal the presence of an oscillatory pattern in the ionization spectra of extreme red (downhill) states that have been kicked away from the ion core (downhill with respect to the potential imposed by the Stark field). We find no oscillations in the spectra of extreme blue (uphill) states that have been kicked towards the ion core (also downhill with respect to the Stark potential). The oscillatory pattern in the red state ionization spectra is explained with a one-dimensional semiclassical model in terms of interferences between two classical paths. This model also predicts that the blue state ionization spectra should also show oscillatory behavior. The absence of the oscillations in the full calculations can be regarded as a breakdown of the one-dimensional model in representing the ionization dynamics of these states. We find that the one-dimensional model fails when the duration of the THz pulse is comparable to the classical Kepler orbit time.

DOI: 10.1103/PhysRevA.68.013405 PACS number(s): 42.50.Hz, 32.80.Fb

I. INTRODUCTION

The physics of ultrafast phenomena has witnessed rapid growth over the past two decades, spurred by major advances in the technology of generating ultrashort electromagnetic pulses. Among the new tools available to experimentalists are sources capable of emitting nearly unipolar electromagnetic pulses, which are generic examples of a ''half-cycle pulse'' (HCP) [1,2]. As pointed out recently, for a freely propagating electromagnetic field the term half-cycle pulse is not strictly correct, since according to the Maxwell's equations, the time integral of the field over the pulse duration must be zero [3]. Measurements of the experimental HCPs [4,5] show them to consist of a short, steep lobe ($\sim$0.5 ps), followed by a long (up to 70 ps) and shallow tail of opposite polarity. Nonetheless, in the interaction between a HCP and a Rydberg atom, when the pulse duration is comparable to or less than the classical electronic orbital period, only the steep initial lobe of the pulse impacts the dynamics of the system [3]. Under these conditions, the HCPs can be approximated accurately as unipolar, ultrafast pulses with a duration τ_{HCP} approximately equal to the duration of the short, steep lobe.

Due to their unipolar nature, the HCPs act as impulsive dc fields that can interact with an atomic electron at any point in its orbit [6]. This is in contrast to conventional photoionization, in which an ac electric field interacts with an electron only near the nucleus. The ability to obtain information about an electron at all points in space has led to a variety of applications of the HCPs. In particular, they have been used to probe the dynamical properties of Rydberg wave packets via experimental techniques such as time-delay spectroscopy [6,7] and impulsive momentum retrieval [8,9]. The HCPs may also prove to be useful tools for quantum control in creating and shaping exotic wave packets [9–15], controlling THz emission from Stark wave packets [16], storing and retrieving information in atomic quantum registers [17,18], and possibly performing selective chemistry in molecules.

A number of experimental and theoretical studies in recent years have focused on the study of excitation and ionization of Rydberg atoms with the HCPs, in regimes in which the duration of the HCP τ_{HCP} is much shorter than or of the order of the Kepler orbital period $\tau_n = 2\pi n^3$, where n is the principal quantum number of the Rydberg state. Due to the particular characteristics of the HCPs, features not observed with conventional laser pulses have been revealed. Examples include broad ionization thresholds and an unconventional $1/n^2$ (or $1/n$ in the impulsive regime limit) scaling law of the ionization threshold field [19,20]. Another feature observed in early studies of Stark states is a manifest asymmetry in the total ionization probability of the uphill (most blue shifted) and downhill (most red shifted) Stark states. The asymmetry can be related directly to the localization of these states with respect to the direction of the applied HCP field [20,21].

In the present study, we investigate in detail the ionization of extreme Stark states of sodium via the half-cycle pulses. For regimes in which $\tau_{\mathrm{HCP}} > \tau_n$, ionization is suppressed [22], whereas for very short pulses $\tau_{\mathrm{HCP}} \ll \tau_n$, the interaction with the core can be neglected, and the electron is simply kicked into the continuum impulsively. Our calculations consider a regime with rich ionization dynamics, in which the duration of the pulse is comparable to the characteristic time of the system $\tau_{\mathrm{HCP}} \simeq \tau_n$.

Depending on the relative orientation between the static electric field $\vec{F}_s$ and the HCP field, one can distinguish two cases. In case one, the HCP field is parallel to the static field, and the electron is kicked downhill (opposite to $\vec{F}_s$). In the second case, the HCP field is antiparallel to the static field, and the electron is kicked uphill (in the $\vec{F}_s$ direction). We concentrate here on the first case, namely, we investigate the ionization of the downhill states kicked downhill (DKD) and the ionization of the uphill states kicked downhill (UKD). We have also performed some calculations for the case where the HCP is antiparallel to the static field. The results indicate that for small static field intensities and most HCP

field strengths, the ionization spectra for the uphill states kicked uphill (UKU) are very similar to those for the DKD, and the ionization spectra for the downhill states kicked uphill (DKU) are similar to those for the UKD. Concentrating on the two cases mentioned above, DKD and UKD, elucidates most of the relevant physics of the problem.

Our analysis shows that the energy resolved ionization spectra of the downhill states display an oscillatory pattern, which appears to have the same origin as the field-dependent oscillations found in earlier studies [23,24]. In contrast, the ionization-energy spectra of the uphill states do not contain any discernible oscillations. We use fully quantum-mechanical calculations to show that the oscillations in the downhill spectrum are strongly influenced by the scaled duration $\tau_{\mathrm{HCP}}/\tau_n$ of the HCP. By employing a mask function that absorbs the electronic flux moving towards the nucleus, we show that interaction with the atomic core is essential in creating the oscillations.

To provide an intuitive, semiclassical picture of the full-quantum results, we perform classical trajectory calculations within the framework of a one-dimensional (1D) model developed previously [25,26]. We find good agreement between the full-quantum and the 1D calculations for the case of ionization of the downhill states. For the uphill states, the quantum and 1D models do not agree. This indicates that the 1D analysis is inadequate, mainly because the electron is not confined to one side of the atom core as implied by the 1D model.

Finally, we examine the spatial evolution of the downhill and uphill states during and following the laser pulse. The results obtained provide support for the applicability of the one-dimensional semiclassical model and the interfering-trajectory method [24,26,27] for the downhill state dynamics, and illustrate how this model fails to explain the uphill ionization dynamics.

II. NUMERICAL METHOD

A. Full-quantum calculations

The Hamiltonian describing the interaction of an HCP with a sodium atom is given by (atomic units are used throughout)

$$H=\tfrac{1}{2}p^2+V(r)+[F_s+F_{\mathrm{HCP}}(t)]z, \tag{1}$$

where F_s and F_{HCP} are the static and the HCP electric fields, respectively (both directed along the $\hat{z}$ axis), and $V(r)$ is a nonlocal pseudopotential for Na, with the following form [28]:

$$V(r)=\sum_l V_l(r)|l\rangle\langle l|+V_{pol}(r)-\frac{1}{r}. \tag{2}$$

In the above expression, $V_l(r)$ is an l dependent, short-range contribution and V_{pol} is a polarization term accounting for the polarization of the core, up to quadrupole contributions. The Hamiltonian preserves azimuthal symmetry, which makes the z component of the angular momentum a constant of motion and m a good quantum number. As a consequence of the finite-sized core of Na, the system is nonseparable in parabolic coordinates, and therefore the parabolic quantum number n_1, which is good for hydrogen, is only approximately good for Na.

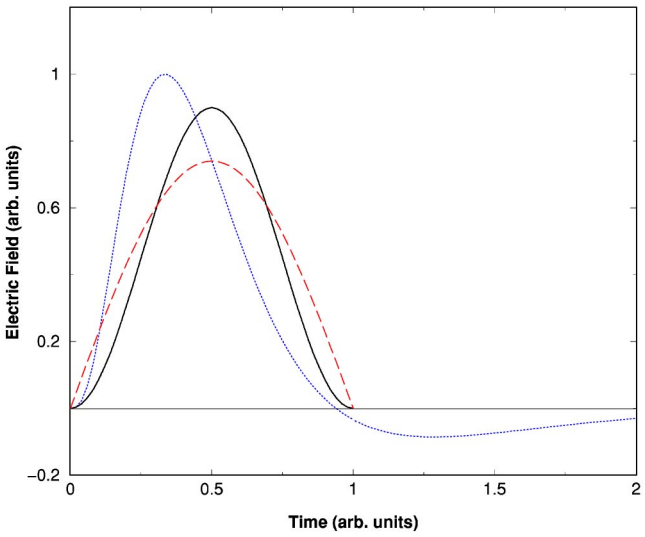

FIG. 1. Theoretical models of the half-cycle pulses: a half-sin^2 form (solid line), half-sin form (dashed line), and a form suggested by Jones (dotted line).

To solve the Schrödinger equation numerically, we employ an expansion of the electronic wave function in spherical harmonics:

$$\Psi(r_j,\theta,t)=\sum_{l=0}^{l_{max}}\Phi_l(r_j,t)Y_l^m(\theta,\phi), \tag{3}$$

where l_{max} is the maximum value of the orbital momentum and r_j's are discrete radial points on a nonuniform radial grid (for details see Ref. [29]). This representation renders an efficient discretization of the problem, with a greater density of radial grid points close to the nucleus and a larger grid spacing far from the core. In this way, an accurate and computationally efficient representation of the time-dependent wave function is achieved. The most important advantage of using the basis representation in Eq. (3) is the sparseness of the Hamiltonian matrix, which becomes tridiagonal in the kinetic and potential terms.

Most of the calculations presented below assume that the HCP has the following form:

$$\vec{F}_{\mathrm{HCP}}(t)=\begin{cases}\hat{\mathbf{z}}F_{\mathrm{peak}}\sin^2\left(\dfrac{\pi}{2\tau_{\mathrm{HCP}}}t\right), & 0\leqslant t\leqslant 2\tau_{\mathrm{HCP}}\\ 0, & t>2\tau_{\mathrm{HCP}},\end{cases} \tag{4}$$

where τ_{HCP} is the full width at half maximum of the electric field and F_{peak} is the maximum amplitude of the HCP. Some tests were also performed using a half-sin form and a form suggested by Jones [21]. The three pulse shapes are displayed in Fig. 1.

In general, our HCP numerical models are justified by the fact that when the duration of the weak tail is much longer than the Kepler period of the Rydberg electron, its effect can

be treated as a small, adiabatic perturbation. In some experiments, even this effect is eliminated by using techniques such as photoswitches to remove the tail [5] and narrow extraction slits to restrict the interaction region [30]. With respect to the influence of the pulse shape on the ionization process, our calculations show that for the same total momentum transfer, the ionization energy spectra for the three pulse shapes, sin, $\sin^2$, and the shape suggested by Jones, are very similar.

In this study, we use initial Stark states of the Na atom with principal quantum numbers $n=15$ through $n=20$. These states are computed by diagonalizing the static field matrix in the unperturbed basis [29]. The initial state is then propagated under the influence of the HCP using a Chebyshev propagator [31]. Since the Chebyshev scheme normally considers time-independent Hamiltonians, and the HCP is a time-dependent field, the total propagation time is divided into equal-length subintervals, with negligible variation in the field during each subinterval. An estimate for the acceptable length of these subintervals is provided by the requirement that they satisfy to a reasonable degree of accuracy the following relation:

$$\int_0^{t_p} F_{\mathrm{HCP}}(t)\,dt = \sum_{i=0}^{N} F_{\mathrm{HCP}}(t_i)\Delta t_i, \tag{5}$$

where t_i are the division points ($t_0=0$, $t_N=t_p$), t_p is the total duration of the pulse, and $\Delta t_i = t_{i+1}-t_i$. The total time propagator is then decomposed as

$$\hat{U}(t_p,0) = \prod_{n=0}^{N-1} \hat{U}(t_{i+1},t_i). \tag{6}$$

This scheme might be further improved by using a division with the subinterval length correlated to the intensity of the time-dependent HCP field. In our calculations, we use equally spaced time divisions ($\Delta t_i = \Delta t$), and we consider between 90 and 120 subintervals per division, which provides for relative errors of less than 0.05% in the final ionization-energy spectrum.

Once a suitable division of the propagation time is found, the Chebyshev scheme is employed in each subinterval. After propagation, the final wave function $|\psi(t_N)\rangle$ is analyzed using an energy window method described previously [32]. Basically, this method projects the wave function onto the positive-energy eigenstates of the field-free Hamiltonian. The result is the ionization probability as a function of the photoelectron energy. In principle, it would be more accurate (and more cumbersome) to project on the eigenstates of the Stark Hamiltonian, rather than the field-free Hamiltonian. However, the error entailed in using the field-free states is roughly $F_s z$. Since most of the calculations in this work use a static field of 400 V/cm, and the average z of the ionized electron is between -600 and 200 a.u., the error is of the order of 10^{-4} a.u. This represents only about 1% of the energy width of the electron after the kick, which is of the order of 10^{-2} a.u.

B. Semiclassical calculations

To provide an intuitive picture of the results obtained by the full-quantum calculations, we have performed a series of classical trajectory calculations within the framework of a one-dimensional model of the Na extreme parabolic states developed previously [25,26]. The full 2D classical Hamiltonian of the system in cylindrical coordinates is given by

$$H_{2D} = \frac{1}{2}\left(p_\rho^2 + p_z^2 + \frac{l_z^2}{\rho^2}\right) - \frac{1}{(\rho^2+z^2)^{1/2}} + V_d[(\rho^2+z^2)^{1/2}] + z[F_s + F_{\mathrm{HCP}}(t)], \tag{7}$$

where l_z is a constant of motion, F_s and $F_{\mathrm{HCP}}(t)$ are the static and the HCP fields, respectively (both parallel to $\hat{z}$), and V_d is the short-range, non-Coulombic contribution of the Na core. Although V_d makes the static field Hamiltonian nonseparable in parabolic coordinates, for states with small quantum defects δ_l ($l \geqslant 2$), this term can be neglected due to the limited penetration of the wave function to the core in these states. Transforming Eq. (7) to semiparabolic coordinates

$$u = (r+z)^{1/2}, \quad v = (r-z)^{1/2}, \tag{8}$$

and extending the phase space (as is customary for time-dependent problems) by introducing the momentum conjugate to time, $p_t = -H(t)$, the Hamiltonian of the system becomes

$$\mathcal{H}_{2D} = \frac{1}{2}\frac{p_u^2+p_v^2-4}{u^2+v^2} + \frac{1}{2}(u^2-v^2)[F_s + F_{\mathrm{HCP}}(t)] + p_t = 0. \tag{9}$$

In the absence of the HCP, the equations of motion for u and v are separable. However, the presence of the time-dependent field couples the two degrees of freedom through the time varying energy $-p_t$. Nevertheless, for initial conditions in which $v=0$ and $p_v=0$, the coupling terms remain zero at all times, and the motion in v can be neglected. Similarly, an approximate separation of the equations of motion for u and v can be performed when the p_v and v coordinates remain small throughout the duration of the HCP [25]. The degree of separability is characterized by a quantity β defined as

$$\frac{p_u^2}{2} + u^2 p_t - 2 + \frac{1}{2}u^4[F_s + F_{\mathrm{HCP}}(t)] = -\left\{\frac{p_v^2}{2} + v^2 p_t - \frac{1}{2}v^4[F_s + F_{\mathrm{HCP}}(t)]\right\} = -\beta. \tag{10}$$

Thus, when the motion in the v coordinate is negligible (small values of β), the system can be described approximately by a 1D Hamiltonian given as

$$\mathcal{H} = \tfrac{1}{2}p_u^2 + u^2 p_t - 2 + \tfrac{1}{2}u^4[F_s + F_{\mathrm{HCP}}(t)] = 0, \tag{11}$$

or in cylindrical coordinates as

$$\mathcal{H}=\frac{p_z^2}{2}-\frac{1}{z}+z[F_s+F_{\mathrm{HCP}}(t)]+p_t=0. \tag{12}$$

Note that in the work of Delos and co-workers [27], an effective nuclear charge, $Z_{eff}=Z-\beta/2$, was used. In this work, we assume $\beta\approx 0$ and take $Z_{eff}=1$.

The above Hamiltonian leads to a system of coupled differential equations, which is integrated using a fifth-order Runge-Kutta algorithm [33]. The results of the integration are in turn used to obtain the final energy manifold of the system. This manifold helps in investigating the properties of the energy-resolved ionization spectrum.

An important point to remember about the 1D model is that the motion of the electron is confined to one side of the nucleus. The electron starts on one side of the core, $z>0$ or $z<0$, and never leaves the half space in which it begins. That is, when the electron scatters from the core, it must backscatter. As a result, in the 1D model uphill states must ionize uphill and downhill states must ionize downhill, regardless of the direction in which the HCP is applied.

III. RESULTS AND DISCUSSION

The existence of localized states is a general feature of systems with highly degenerate manifolds under the influence of an external interaction [34,35]. For the case of the sodium atom, a moderate external electric field mixes the quasidegenerate $l\geqslant 2$ states (the *s* and *p* states are split off by large quantum defects) with the same magnetic number *m* in a given *n* manifold, to form a Stark manifold. As in hydrogen, the states in the Stark manifold are labeled by the quantum number *k*, which, for a given principal quantum number *n*, takes the values $n-3,n-5,\ldots,-n+3$ [36]. The interaction with the external electric field lifts the orbital angular-momentum degeneracy and induces a pronounced localization of the extreme Stark states, as shown in Fig. 2.

The red-shifted states are characterized by an electric dipole moment parallel to the external field (directed along the *z* axis), as a consequence of their localization along the $-z$ axis. Viewing the external potential $+F_s z$ as a potential rising monotonically in the direction of the $+z$ axis, these states are termed downhill states. The blue-shifted states (higher energy) are termed uphill states, and are localized along the $+z$ axis, with a dipole moment antiparallel to the external field.

One effect of the localization of the extreme Stark states is the manifest asymmetry in the total ionization rates for the uphill and downhill states [20,21]. The downhill states are easier to ionize, since the electronic wave function in these states is localized mainly along the negative *z* axis, close to the saddle point of the combined Coulomb and Stark potentials. As a result, the electron can be easily kicked over the potential barrier by the HCP field. In contrast, the wave functions of the uphill Stark states are localized on the opposite side of the nucleus ($z>0$), and the HCP electric field pushes the electron towards a collision with the atomic core. The scattering from the core reduces the total-energy transferred by the HCP, which makes ionization more difficult. We find that with very small momentum transfers, ionizing an uphill state is actually easier than ionizing the downhill state. This observation has also been verified in experiments [1]. Further studies are underway to determine the physical origin of this effect.

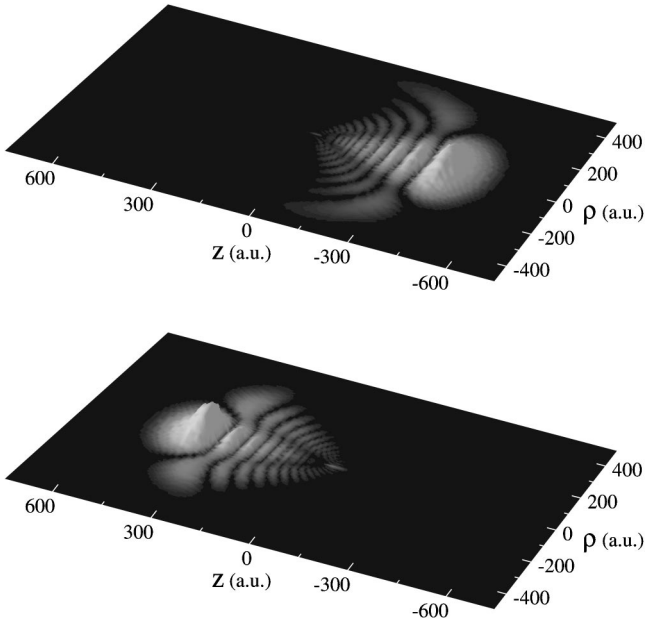

FIG. 2. Plots of the electronic distributions for $n=15$, $k=-12$ (top), and $k=+12$ (bottom) Stark states.

As in previous studies [23,24], we first investigate the dependence of the total ionization rate on the peak amplitude of the HCP field. The results of our calculations are presented in Fig. 3. For the downhill state the figure shows oscillations in the total ionization rates, whereas for the uphill state no oscillations are present. To analyze the oscillations in greater detail, we consider the derivative of the curve in Fig. 3 (see Fig. 4). The quantity dI/dF_{peak} (F_{peak} is the peak intensity of the HCP) can be related to the threshold

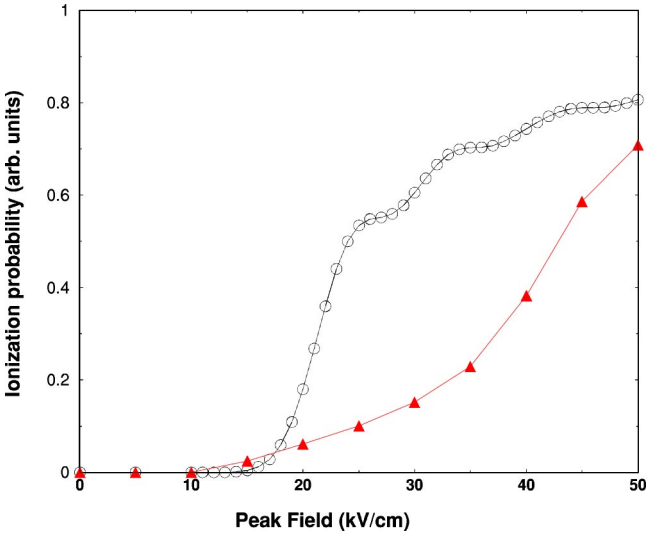

FIG. 3. Total ionization probability for Na $n=15$ stark states ($F_s=400$ V/cm) kicked downhill by a $\sin^2$ HCP with $\tau_{\mathrm{HCP}}=400$ fs ($k=+12$, filled triangles; $k=-12$, open circles).

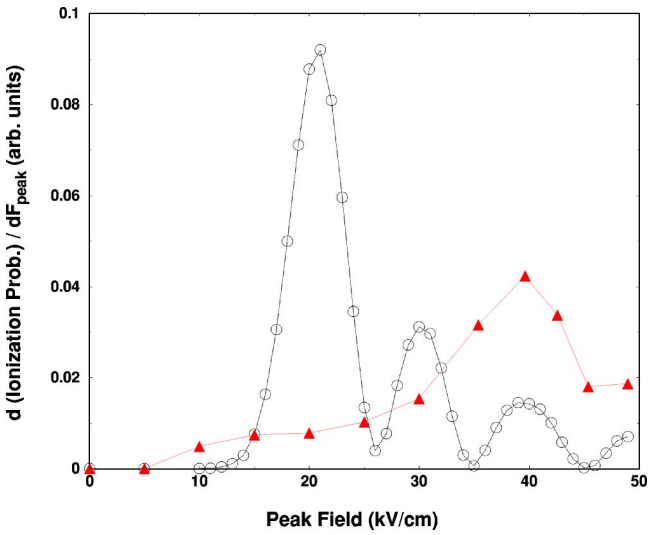

FIG. 4. Derivative of the total ionization probability in Fig. 3 with respect to the peak intensity of the HCP ($k=+12$, filled triangles; $k=-12$, open circles).

ionization probability $P(E=0)$ for fixed pulse length as follows:

$$\frac{dI}{dF_{\text{peak}}} \propto \frac{dI}{dQ} \propto P(E=0), \tag{13}$$

where $Q=\int_0^{t_p} F_{\text{HCP}}(t)dt$ is the total momentum transfer of the pulse. Hence, the oscillations in the total ionization rates are related to the oscillations expected in experiments measuring the threshold ionization probability.

The energy-resolved ionization spectra for the uphill and downhill states can be obtained using the window method discussed previously [32]. Figure 5 shows the $k=-12$ downhill (DKD) and $k=+12$ uphill (UKD) ionization spectra for sodium $n=15$, $m=0$ states, after interaction with a $\sin^2$ HCP ($F_{\text{peak}}=160$ kV/cm, $\tau_{\text{HCP}}=100$ fs, $Q=0.129$ a.u.) directed along the $+z$ axis. A striking difference is displayed in the results for these two cases. The DKD spectrum shows oscillations in the final energy probabilities, whereas the UKD spectrum lacks any discernible oscillations. These results suggest that the oscillations in the total ionization rates observed for the downhill state are in fact related to the oscillatory pattern present in the ionization-energy spectrum.

To provide an intuitive, semiclassical explanation of the oscillations in the DKD ionization spectrum, we employ the one-dimensional semiclassical model described above. This model explains the oscillations in terms of two interfering trajectories. To illustrate the predictions of this model, we have performed classical trajectory Monte Carlo calculations [37,38] that show the evolution of the initial energy manifold during the HCP. As in an earlier study [26], we start with a number of trajectories uniformly distributed in the angle variable $\theta_n=\phi_e-\sin\phi_e$, where ϕ_e represents the so-called eccentric anomaly of the electron orbit. The initial values for z and p_z are then given by $z=n^2(1-\cos\phi_e)$, $p_z=n\sin\phi_e/z$. For each of the above trajectories, we integrate

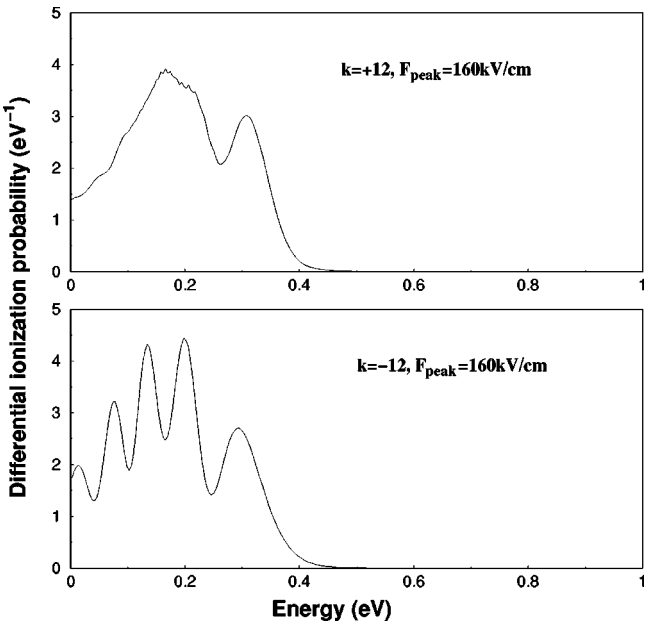

FIG. 5. Ionization spectra for Na $n=15$ Stark states ($F_s=400$ V/cm) excited by a $\sin^2$ HCP with $Q=0.129$ a.u. and $\tau_{\text{HCP}}=100$ fs. The top panel shows the spectrum for $k=+12$ (uphill) state and the bottom panel shows the spectrum for $k=-12$ (downhill) state.

the classical equations of motion to determine the final energy of the electron. The results are shown in Fig. 6. Since the energy is a periodic function in the angle variable, it is clear that for any energy in the final manifold (except for the extrema) there are exactly two trajectories with that energy. As a result, any horizontal line corresponding to a particular final energy crosses the manifold at two points, and the corresponding θ_i's of these two points are the initial angle variables of the two trajectories reaching that final energy.

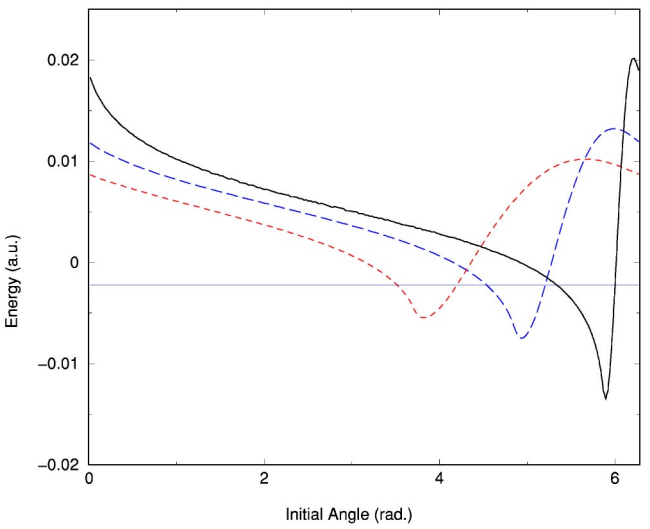

FIG. 6. Final energy manifolds for a HCP of $Q=0.129$ a.u.: $\tau_{\text{HCP}}=25$ fs (solid line); $\tau_{\text{HCP}}=100$ fs (dashed line); and $\tau_{\text{HCP}}=200$ fs (dotted line). The initial energy manifold is denoted with a horizontal solid line.

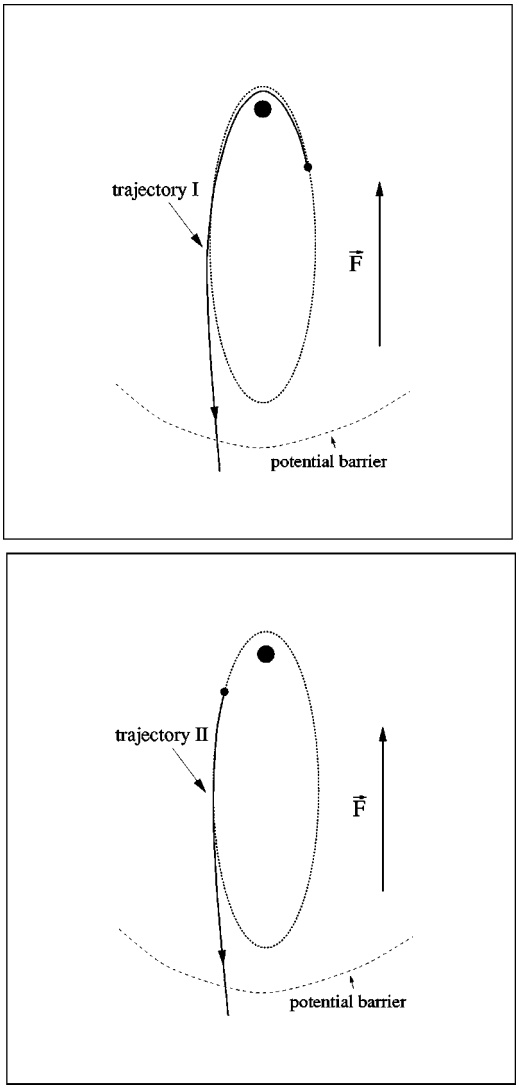

FIG. 7. Schematic of two interfering trajectories. The force acting on the electron is directed opposite to the electric field $\vec{F}$.

Figure 7 shows a schematic of two classical trajectories interfering to produce oscillations in the energy spectra. In one trajectory, the electron moves initially towards the core, and loses energy as it opposes the HCP field. After rebounding from the core, the electron gains enough energy to escape over the barrier to ionization. In trajectory II, the electron initially moves away from the nucleus, antiparallel to the electric field, and gains energy continuously until it ionizes. Although the electron in the first trajectory initially loses energy, after the rebound, the loss is compensated for by the large energy transfer due to the high momentum in the vicinity of the nucleus $(E=-\int \vec{F}_{\mathrm{HCP}}\cdot\vec{v}_e dt)$. Eventually, for proper initial conditions, the electron in trajectory I achieves the same final energy as the electron in trajectory II. Semiclassically, the quantum wave functions associated with the two trajectories interfere to produce the oscillatory pattern in the ionization spectrum. The above model suggests that the short-range interaction with the core plays a key role in the ionization dynamics.

To study the influence of the core in the quantum calculations, we implement a smooth absorbing mask function, to remove the electronic flux moving towards the nucleus. As can be seen in Fig. 8, as the mask function becomes more effective in eliminating the component of the wave function interacting at close range with the nucleus (that is, as the mask function radius increases), the interference pattern disappears. This result shows that the close-range interaction with the core is essential to produce the interference pattern, and is consistent with the predictions of the semiclassical analysis.

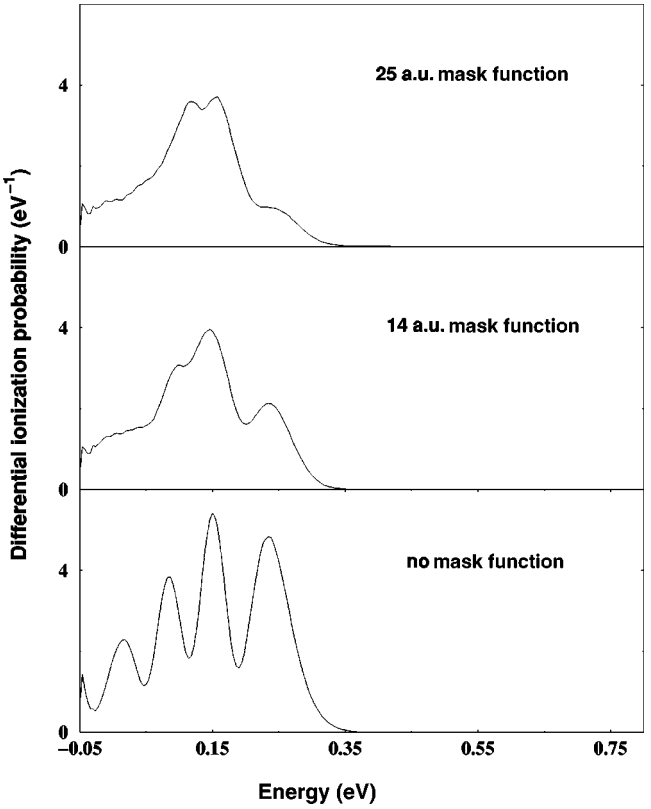

FIG. 8. Ionization spectra for sodium $n=15$, $k=-12$ hit by a HCP with $Q=0.129$ a.u. and $\tau=200$ fs. As the size of the flux mask function increases, the oscillations diminish.

Another aspect of the quantum results that is in accord with the one-dimensional semiclassical model is the dependence of the ionization spectrum on the HCP pulse length τ_{HCP}. When the pulse length is much shorter than the Kepler period $\tau_{\mathrm{HCP}}\ll\tau_n$, the electron does not have sufficient time to interact with the core while the pulse is on, and the net effect is a simple ''kick'' of the electron, with a transferred impulse $Q=-\int_0^{t_p}F_{\mathrm{HCP}}(t)dt$. In this ''impulse approximation,'' the wave function for the electron after the interaction with the HCP is related to the wave function before the interaction by

$$\psi_f(\vec{r})=e^{iQz}\psi_0(\vec{r}). \tag{14}$$

One can easily show, using a Fourier expansion of the initial wave function in momentum space, that the energy transferred during the interaction is

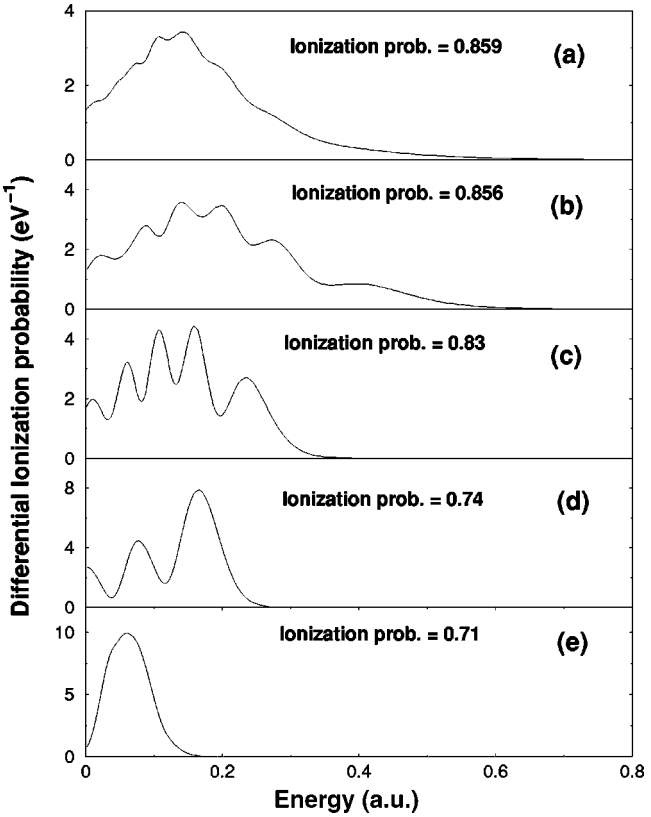

FIG. 9. Ionization spectra and total ionization probability for sodium, $n=15$, $k=-12$ ($F_s=400$ V/cm) hit by a $\sin^2$ HCP of $Q=0.129$ a.u. as a function of the pulse duration: (a) impulsive limit, $\tau_{\mathrm{HCP}}=0$ fs; (b) $\tau_{\mathrm{HCP}}=25$ fs; (c) $\tau_{\mathrm{HCP}}=100$ fs; (d) $\tau_{\mathrm{HCP}}=400$ fs; and (e) $\tau_{\mathrm{HCP}}=800$ fs.

$$\Delta E=\frac{p_f^2}{2}-\frac{p_i^2}{2}=p_{iz}Q+\frac{Q^2}{2}, \tag{15}$$

where p_i and p_f are the initial and final average momenta, and p_{iz} is the average of the z component of the momentum over the initial wave function. As an example, Fig. 9(a) shows the spectrum resulting from the final wave function $e^{iQz}\psi_0(\vec{r})$, with ψ_0 corresponding to the $n=15$, $k=-12$ downhill state of Na, and $Q=0.129$ a.u. The spectrum is computed using a Chebyshev polynomial expansion of the exponential. Readily apparent in Fig. 9(a) is that the oscillations in the spectrum disappear in the impulsive limit. Semiclassically, this can be related to the fact that the transition amplitudes corresponding to the two interfering trajectories are proportional to $|\partial I_f/\partial\theta_i|^{-1}$ (or $|\partial E_f/\partial\theta_i|^{-1}$) [27], where

$$\langle I_f|I_0(t)\rangle=\left(-2\pi i\frac{\partial I_f}{\partial\theta_i}\right)^{-1/2}\times\exp\left[i\int_{t_0}^{t_f}\left(-\theta(t)\frac{dI}{dt}-H(t)\right)dt\right]. \tag{16}$$

In the limit of ultrashort pulses, one can see in Fig. 6 that the quantity $|\partial E_f/\partial\theta_i|^{-1}$ approaches 0 (∞ slope) for the trajectories on the right branch ($\theta_0>\theta_{min}$, where θ_{min} corresponds to the trajectory with minimum final energy) of the final manifold. As a result, one of the two trajectories has a much smaller transition amplitude than the other, and the interference is greatly reduced. Intuitively, the lack of oscillations in the spectra calculated in the impulsive limit spectrum can be related to the fact that the electron does not have time to interact with the core while the HCP is on. Therefore, the two-trajectory interference mechanism described above is not operative.

As the HCP pulse length increases, the oscillations in the ionization spectrum become more evident, and the frequency of the oscillations increases slightly towards higher energies. This can also be related to the classical calculations, in which for longer pulses, the final manifold tends to be more symmetric around the minimum value. As a result, the slope of the trajectories on the right branch ($\theta_0>\theta_{min}$) becomes comparable to the slope of the trajectories on the left branch ($\theta_0<\theta_{min}$), and the corresponding transition amplitudes of the two branches have more similar values. This causes the oscillatory interference patterns to display greater contrast [see Figs. 9(b) and 9(c)].

Another fact apparent in the spectra in Figs. 9(b) and 9(c) is a decrease in the total ionization probability as the pulse length increases (at constant Q). Unlike the case of impulsive excitation, the interaction with the core becomes more important as the pulse gets longer. Since the effect of this interaction is to slow and curve the trajectory of an electron moving away from the nucleus, the total-energy transferred from the pulse, $\Delta E=-\int_0^{t_p}\vec{F}_{\mathrm{HCP}}(t)\cdot\vec{v}_e dt$, is reduced considerably. A more significant reduction of the total ionization probability is observed when $\tau_{\mathrm{HCP}}>\tau_n/2$ [Fig. 9(d)]. This decrease is expected, since, on an average the interaction time of the electron with the core is $\tau_n/2$. The frequency of the oscillations also decreases, which can be related to a decrease in the speed of variation with energy of the phase difference between the two interfering paths, $\delta(\Delta\phi)/\delta E$.

While the DKD case is well described by the one-dimensional semiclassical model, the UKD case is not. In particular, the same argument of periodicity in the final energy manifold would predict that spectral oscillations will also be present in the UKD spectra. However, the full-quantum calculations show no oscillations in the UKD case.

An examination of the electronic wave functions for the Na, $n=15$, $m=0$ downhill ($k=-12$) and uphill ($k=+12$) states as they propagate under the influence of the HCP (Fig. 10), reveals a marked difference between the spatial evolution of the two states. For the uphill state, an important part of the wave function is pushed by the HCP field past the atomic core, into the $-z$ region. The electron wave function is strongly scattered by the short-range interaction with the core. In contrast, the downhill state remains at all times in the same half space ($z<0$) in which it started, and shows a much smoother and quasi-1D evolution towards the asymptotic regions of the grid.

A more revealing depiction of the differences between the UKD and DKD cases can be seen by analyzing the wave packet evolution in semiparabolic coordinates, u and v [cf. Eq. (8)]. Figure 11 displays the averages of the u and v

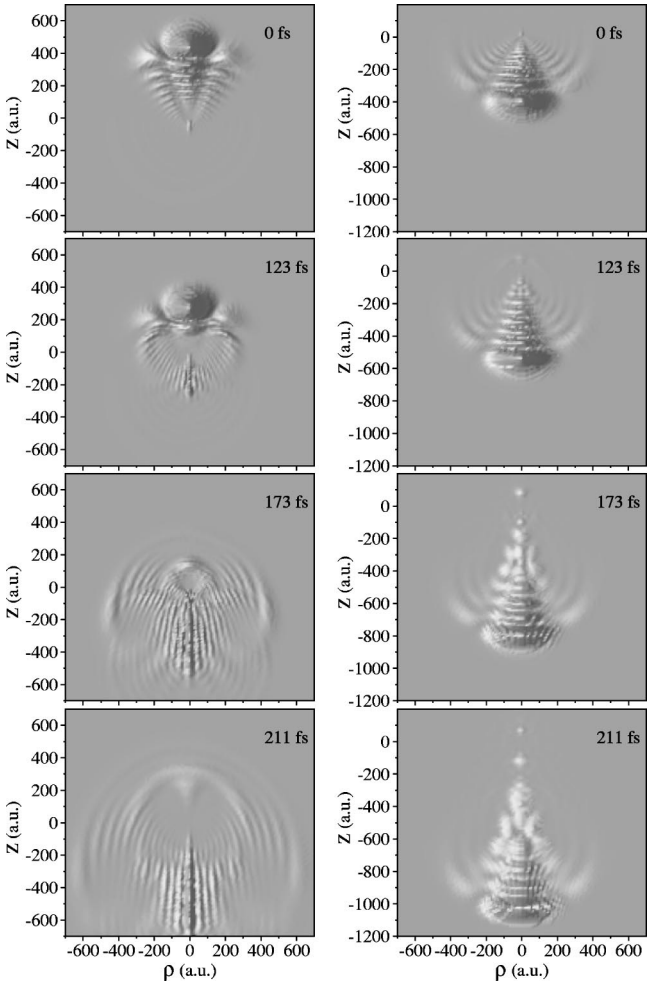

FIG. 10. Electronic distribution as a function of time during the interaction with a $\sin^2$ HCP of $Q=0.129$ a.u. and $\tau_{\mathrm{HCP}}=100$ fs. The panels on the left display the evolution for $k=+12$ uphill state and the panels on the right show the evolution of $k=-12$ downhill state.

coordinates computed from the time-dependent electronic wave functions. While the motion of the downhill state in the v coordinate is negligible, the uphill state displays significant development in this coordinate. Since the 1D model requires quasi-one-dimensional dynamics at all times [Eq. (10)], it is clear that this model is inadequate to describe the ionization of the uphill states (when kicked downhill). As a result, the semiclassical, two-trajectory model is not applicable. The emergence of a second dimension in the problem transforms the final energy manifold into a 3D surface depending on two parameters. The intersection of the final manifold with a constant energy plane is a contour in the plane (instead of only two points in the 1D case). Consequently, multiple trajectories will have the same final energy, and their noncorrelated contributions will tend to cancel out, leading to the destruction of the oscillatory interference pattern.

The evolution of the uphill state in the v coordinate (as observed in Fig. 11) is primarily due to the fact that, during the interaction with the HCP, most of the uphill wave function penetrates beyond the core, into the $-z$ region. As Fig. 12(a) shows, for short pulses, the downhill ionization flux is

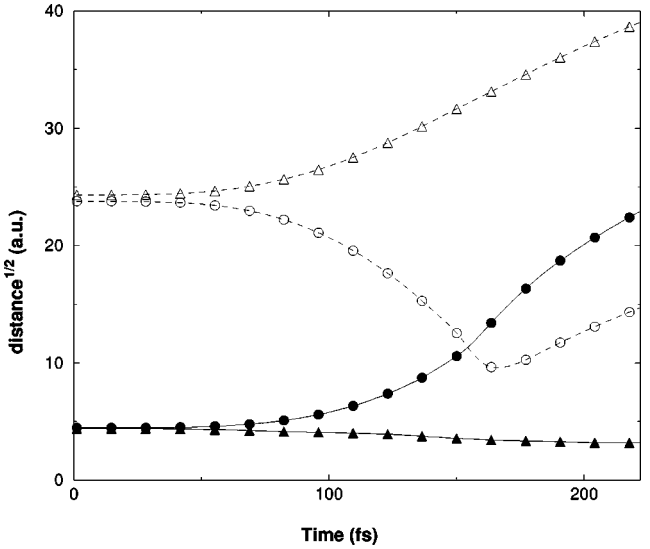

FIG. 11. Evolution of the expectation values of the semi parabolic coordinates during the interaction with a $\sin^2$ HCP of $Q=0.129$ a.u. and $\tau_{\mathrm{HCP}}=100$ fs. The solid lines show the expectation value of v for the uphill (filled circles) and downhill (filled triangles) states. The dashed lines show the expectation value of u for the uphill (open circles) and downhill (open triangles) states.

considerably larger than the uphill flux, and the electron has a high probability of ionizing, as expected, in the $-z$ direction. For weaker pulses (lower Q's) of durations comparable to the Kepler orbital period ($\tau_{\mathrm{HCP}}\simeq\tau_n$), the probability for the uphill electron to scatter past the nucleus decreases, and the electron has a higher probability (although small in absolute value) to ionize in the $+z$ direction [21] [see Fig. 12(b)].

Under conditions in which the penetration of the wave function into the $-z$ region is reduced, the motion in v is limited, and the 1D model is adequate, at least qualitatively. Consequently, one would expect to observe oscillations in the final energy spectra [although only in the bound spectrum since the ionization probability would be very small, see Fig. 13(a)]. Calculations also show that, for the same external pulse, the hydrogen uphill states are less likely to penetrate beyond the core in the $-z$ direction than their sodium counterparts. This difference is a result of the nonzero coupling between the sodium blue and red states, due to the finite size of the core [36]. In effect, the 1D approximation is more accurate in describing the evolution of the hydrogen uphill state, and the final spectrum displays oscillations with greater contrast [again, only in the bound spectrum, see Fig. 13(b)].

The results and interpretation presented above indicate that the condition necessary to observe interference oscillations in the uphill case (UKD) is that the uphill dynamics are constrained to the $+z$ region. Since the part of the uphill wave function localized along the $+z$ axis is primarily scattered back into the $+z$ region by the core, the 1D approximation should be fairly accurate in describing its dynamics. The final energy spectrum, obtained when the analysis of the final wave function is restricted to the region $0<\theta<\pi/25$ rad [see Fig. 13(c)], confirms this hypothesis.

The importance of the quasi-one-dimensional dynamics of

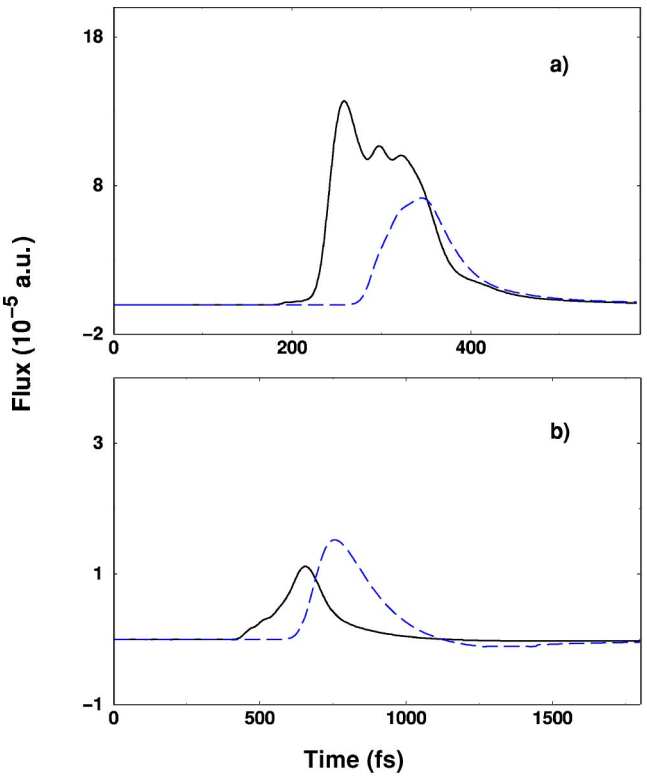

FIG. 12. Asymptotic electronic flux through the right and left hemispheres of a 920 a.u. radius sphere, centered at the origin. Panel (a) shows a sodium $n=15$, $k=+12$ state ionized by a $\sin^2$ HCP with $\tau_{\mathrm{HCP}}=100$ fs and $F_{\mathrm{peak}}=160$ kV/cm and panel (b) shows the same state ionized by a $\sin^2$ HCP with $\tau_{\mathrm{HCP}}=282$ fs and $F_{\mathrm{peak}}=26.5$ kV/cm. In both panels, the flux ionizing downhill is shown by the solid line and the flux ionizing uphill is shown by the dashed line.

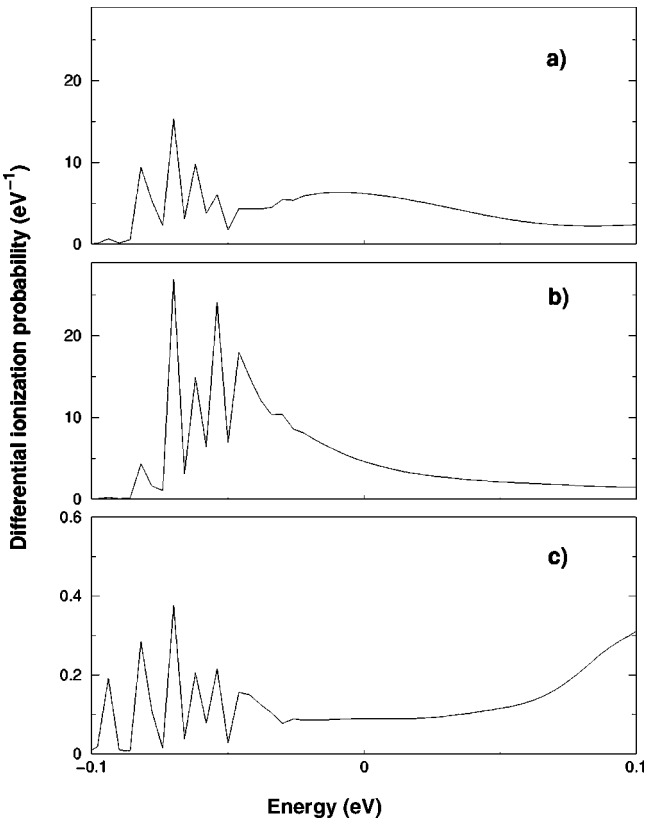

FIG. 13. Final energy spectra: (a) sodium, $n=15$, $k=+12$ state hit by $\sin^2$ HCP, $\tau_{\mathrm{HCP}}=300$ fs, $F_{\mathrm{peak}}=56$ kV/cm; (b) hydrogen, $n=15$, $k=+14$ hit by $\sin^2$ HCP, $\tau_{\mathrm{HCP}}=300$ fs, $F_{\mathrm{peak}}=56$ kV/cm; (c) restriction to $0<\theta<\pi/25$ for the final wave function of Na $n=15$, $k=+12$ hit by $\sin^2$ HCP, $\tau_{\mathrm{HCP}}=200$ fs, $F_{\mathrm{peak}}=80$ kV/cm.

the wave function for the observation of interference effects is also demonstrated in the dependence of the ionization spectrum on the static field magnitude (see Fig. 14). The static field is essentially an alignment mechanism that provides the initial localization of the electronic wave function along the z axis. At very low fields, the 15d state, due to its small quantum defect, is not yet mixed with the higher-l states in the Stark manifold. As a result, the state that would be $k=-12$ (the downhill state), has nearly pure d ($l=2$) character, and is not well localized along the z axis. During the interaction with the HCP, this produces sufficient motion in the semiparabolic v coordinate to break the quasi-1D dynamics.

As the magnitude of the static field increases (100 V/cm and higher), the 15d state joins the Stark manifold and becomes the $k=-12$ Stark state. The confinement of this state along the z axis becomes more pronounced, and the 1D approximation is valid [Eq. (10)]. Consequently, oscillations, as predicted by the 1D model, are evident in the ionization-energy spectrum.

IV. CONCLUSIONS

In conclusion, this work presents a detailed study of oscillations in the ionization spectrum of a Stark state in so-

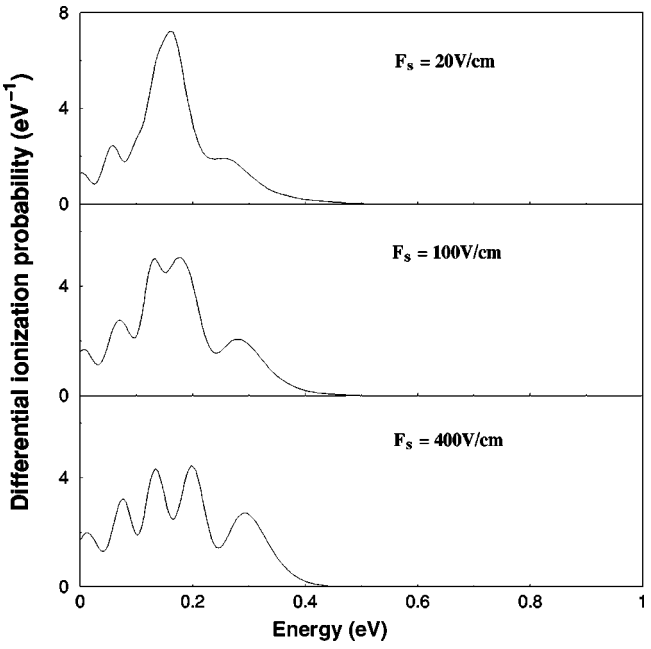

FIG. 14. Ionization spectra for Na $n=15$, $k=-12$ hit by a $\sin^2$ HCP ($\tau_{\mathrm{HCP}}=100$ fs, $F_{\mathrm{peak}}=160$ kV/cm) as a function of the static electric field F_s.

dium excited by a half-cycle pulse. Full-quantum calculations revealed oscillations in the DKD spectrum that can be explained with a 1D semiclassical model as interference effects between two dominant trajectories leading to the same final energy. The UKD spectra, on the other hand, showed no oscillations, due to a larger angular spread of the wave function as it scatters from the core, which implies the contribution of many noncorrelated paths to the same final energy. To isolate the role of the atomic core during the interaction with the HCP, we employed a flux mask function to remove the electronic flux near the core. For the downhill state, we also investigated the dependence of the oscillations on the length of the pulse and related the results to predictions of the semiclassical theory. We demonstrated that the good agreement between our results and the 1D semiclassical model for the downhill states is due to the quasi-1D dynamics of these states. Finally, we showed that the one-dimensional model is not adequate for describing the uphill ionization, due to significant evolution of the uphill states in the v semiparabolic coordinate. This motion results from the scattering of the uphill states beyond the core, as they are pushed in the $-z$ direction by the HCP field. The resulting, quasi-2D ionization dynamics of the uphill states suppresses the oscillations in the UKD spectra.

ACKNOWLEDGMENTS

This work was partially supported by the National Science Foundation through Grant No. CHE-9875080. K.J.S. acknowledges support from the Danish-American Fulbright Foundation and the National Science Foundation through Grant No. PHY-9733890.

[1] R.R. Jones, D. You, and P.H. Bucksbaum, Phys. Rev. Lett. **70**, 1236 (1993).
[2] G.M. Lankhuijzen and L.D. Noordam, Phys. Rev. A **52**, 2016 (1995).
[3] C. Wesdorp, F. Robicheaux, and L.D. Noordam, Phys. Rev. Lett. **87**, 083001 (2001).
[4] D. You, R.R. Jones, D. Dykaar, and P. Bucksbaum, Opt. Lett. **18**, 290 (1993).
[5] N.E. Tielking, T.J. Bensky, and R.R. Jones, Phys. Rev. A **51**, 3370 (1995).
[6] C. Raman, C.W.S. Conover, C.I. Sukenik, and P.H. Bucksbaum, Phys. Rev. Lett. **76**, 2436 (1996).
[7] C. Raman, T.C. Weinacht, and P.H. Bucksbaum, Phys. Rev. A **55**, R3995 (1997).
[8] M.B. Campbell, T.J. Bensky, and R.R. Jones, Phys. Rev. A **58**, 514 (1998).
[9] R.R. Jones, Phys. Rev. Lett. **76**, 3927 (1996).
[10] C.O. Reinhold, J. Burgdörfer, M.T. Frey, and F.B. Dunning, Nucl. Instrum. Methods Phys. Res. B **132**, 316 (1997).
[11] M.T. Frey, F.B. Dunning, C.O. Reinhold, and J. Burgdörfer, Phys. Rev. A **55**, R865 (1997).
[12] C.O. Reinhold, J. Burgdörfer, M.T. Frey, and F.B. Dunning, Phys. Rev. A **54**, R33 (1996).
[13] N.E. Tielking and R.R. Jones, Phys. Rev. A **52**, 1371 (1995).
[14] J. Ahn, D.N. Hutchinson, C. Rangan, and P.H. Bucksbaum, Phys. Rev. Lett. **86**, 1179 (2001).
[15] M. Klews and W. Schweizer, Phys. Rev. A **64**, 053403 (2001).
[16] K.J. Schafer and J.L. Krause, Opt. Express **1**, 210 (1997).
[17] J. Ahn, T.C. Weinacht, and P.H. Bucksbaum, Science **287**, 463 (2000).
[18] C. Rangan and P.H. Bucksbaum, Phys. Rev. A **64**, 033417 (2001).
[19] C.O. Reinhold, M. Melles, H. Shao, and J. Burgdörfer, J. Phys. B **26**, L659 (1993).
[20] R.R. Jones, N.E. Tielking, D. You, C. Raman, and P.H. Bucksbaum, Phys. Rev. A **51**, R2687 (1995).
[21] A. Bugacov, B. Piraux, M. Pont, and R. Shakeshaft, Phys. Rev. A **51**, 4877 (1995).
[22] C. Rangan, K.J. Schafer, and A.R.P. Rau, Phys. Rev. A **61**, 053410 (2000).
[23] C.O. Reinhold, J. Burgdörfer, R.R. Jones, C. Raman, and P.H. Bucksbaum, J. Phys. B **28**, L457 (1995).
[24] C.O. Reinhold and J. Burgdörfer, Phys. Rev. A **51**, R3410 (1995).
[25] C.D. Schwieters and J.B. Delos, Phys. Rev. A **51**, 1023 (1995).
[26] M. Mallalieu and S.I. Chu, Chem. Phys. Lett. **258**, 37 (1996).
[27] C.D. Schwieters and J.B. Delos, Phys. Rev. A **51**, 1030 (1995).
[28] J.N. Bardsley, in *Case Studies in Atomic Physics*, edited by E.W. McDaniel and M.R.C. McDowell (North-Holland, Amsterdam, 1975), Vol. IV, pp. 302–368.
[29] J.L. Krause and K.J. Schafer, J. Phys. Chem. **103**, 10 118 (1999).
[30] D. You and P.H. Bucksbaum, J. Opt. Soc. Am. B **14**, 1651 (1997).
[31] H. Tal-Ezer and R. Kosloff, J. Chem. Phys. **81**, 3967 (1984).
[32] K.J. Schafer, Comput. Phys. Commun. **63**, 427 (1991).
[33] S.E. Koonin, *Computational Physics* (Benjamin/Cummings, Mento Park, CA, 1986).
[34] A.R.P. Rau, Phys. Rev. Lett. **63**, 244 (1989).
[35] A.R.P. Rau, J. Phys. B **27**, 2719 (1989).
[36] T.F. Gallagher, *Rydberg Atoms* (Cambridge University Press, Cambridge, 1994).
[37] R. Abrines and I.C. Percival, Proc. Phys. Soc. Jpn. **88**, 861 (1966).
[38] I.C. Percival and D. Richards, Adv. At. Mol. Phys. **11**, 1 (1975).